The influence of history effects on the diffusion-driven dissolution of CO$_2$ bubbles

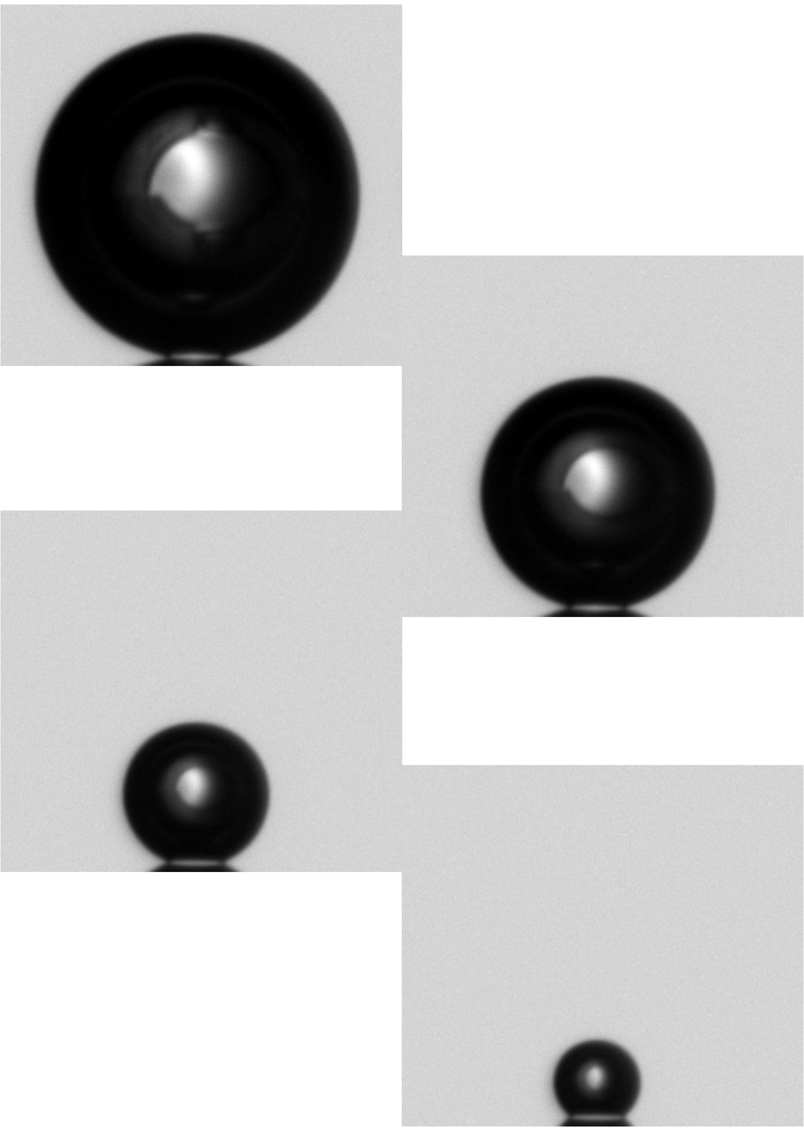

Prof. Dr. Devaraj van der Meer
Dr. Oscar R. Enríquez

Carlijn I. van Emmerik

UNIVERSITY OF TWENTE.

Physics of Fluids

Summary

In this research the growth and dissolution process of a CO_2 bubble in a CO_2-water solution was investigated. The bubble grew at slightly oversaturated conditions and we were particularly interested in the bubble dissolution under different saturation conditions.

The experiments were done in a controlled environment where a bubble grew from a cavity with a pre-existing gas pocket when the CO_2-water solution was made slightly oversaturated. The bubbles were of a micrometer scale and the process was visualised using a camera with a microscope objective. The dissolution was induced by a change in saturation condition from oversaturated to saturated, under- or marginally oversatured.

A theoretical relation was derived to describe the growth and dissolution of a bubble under those changing conditions. The experimental results are compared with numerical simulations of this relation. However, the comparisons did not show full agreement for several reasons that we explore in this work. One explanation is that convection was neglected in the derivation of the theory. Even though convection was not dominant over diffusion it could have influence on the results. Another explanation is that the simulations are based on several choices and assumptions, which were especially critical for the dissolution of a bubble under saturated conditions.

Contents

Chapter 1

Introduction

Bubble formation and dissolution takes place in every day life around you. As a kids we enjoy the beauty of soap bubbles and the foam in bath. Various studies have been done on the behaviour of foam for industrial applications [1, 2]. People who have a aquarium with tropical fishes have a column of bubbles inside to ensure that their is enough oxygen in the water. Bubbles that develop when a waves breaks on the shore are important for the air-sea gas exchange of oceans [3]. Examples of bubble formation due to chemical reactions are electrolysis [4] to obtain gasses from solutions and cakes become spongy due to the combination of acid and backing soda. Cavitation of bubbles can cause damage to a ship due to cavitation of bubbles around the propeller blades [5, 6] whereas mantris shrimps use bubble cavitations to catch their prey [7].

From the previous examples it can be clear that the research to the growth, dissolution and stability of gas bubbles in a gas-liquid solution is of great interest for several applications. Bubble growth under oversaturated conditions can occur in the blood or tissues of people with decompression sickness [8] and diving protocols are changed to limit bubble formation and growth due to hyperbaric decompression [9]. The dissolving properties of undersaturated conditions are relevant for artificial oxygen carriers that transport oxygen from lungs to tissue [10, 11]. In several industrial applications bubbles arise in the production process, (e.g. during oil extraction, the production of ice cream [12] or glass) where sometimes, for an optimal product or process, those bubbles have to be removed by dissolution.

Carbonated beverages, champagnes and beer are examples of gas-liquid solutions in every day life. Those drinks have a moderate supersaturation of gas which will escape if they are left open and hence allowed to go ‘flat’. Most of the gas will escape through the free surface by diffusion but also bubbles will form when nucleation sites are present. Nucleation sites in those drinks are for example minuscule scratches or tiny particles that are stuck on the glass surface (e.g. bubbles in a glass of champagne) [13, 14]. Bubbles grow also from porous media as during oil extraction and in elastomers [15].

The question how surface nanobubbles can be stable for hours or even days is still under debate. The stability can be partly caused by the fact that the surrounding liquid is close to its saturation value [16, 17, 18]. Therefore the gas bubbles that are grown under slightly oversaturated conditions are dissolved (or stabilized) under saturated, under- or marginally oversaturated conditions which can help to get better insight in the bubble behaviour. Our experiments are done with bubbles on micrometer scale because they can be visualized, have similar behaviour as nanobubbles and the fluid dynamical equations that are used to describe the growth/dissolution process are all valid down to nanometer scale.

In the experiments that have been carried out so far [13, 19] the flow induced by the growing bubble on its surrounding was perhaps not completely negligible. In this research we want to investigate the growth of bubbles dominated by diffusion as mass transfer mechanism. Therefore the growth of the bubbles took place under slightly oversaturated condition described by Enríquez et al. [20] to ensure a quasi-static growth. They also gave a prediction of the time where natural convection becomes patent [21, p. 49]. In this research the onset time of natural convection is taken into account because convection will have influence on the growth and dissolution of a bubble. In order to mimic realistic situations, the gas bubbles where grown on a solid impermeable substrate submerged in a gas-liquid solution.

Epstein and Plesset derived relations to describe the growth or dissolution of a spherical gas bubble in a infinite respectively over- or undersaturated solution [22]. Those equations are used in experimental and numerical situations [18, 23] and to investigate the contribution of surface tension and saturation conditions during dissolution [24]. The derivation of the Epstein Plesset equations is used as guideline to obtain a relation that describes the growth and dissolution dynamics of the bubble related to the environmental concentration changes in this research.

Chapter 2

Introducing experimental properties

In this research the main focus was on the dissolution of a bubble that first has grown under slightly oversaturated and then dissolves under undersaturated conditions in a gas-liquid solution. In this chapter the definition of over- and undersaturation will be given. Finally the process will be described to make the gas-liquid solution over- and thereafter undersaturated and the corresponding change of the physical properties of the gas bubble will be explained.

2.1 Over- and undersaturation

Henry's law describes that at a constant temperature, T, the equilibrium (saturation) concentration, C, of gas dissolved in a liquid is proportional to the partial pressure, P, of the gas above the liquid:

$$C = k_H(T)P, \tag{2.1}$$

Here k_H is Henry's coefficient which is a decreasing function of temperature and is specified for each gas-liquid pair.

Initially the gas liquid solution is saturated at a concentration C_I. This concentration is established in thermodynamic equilibrium at a pressure P_I and a temperature T_I. The solution will be oversaturated when the pressure is brought to a lower pressure P_S, and/or the temperature is raised to a higher temperature T_S. In this case there is more gas dissolved than could be at equilibrium under the new conditions. Therefore gas will escape from the solution in order to establish the new equilibrium at $C_S = k_H(T_S)P_S$. On the other hand, when the solution is undersaturated it will absorb gas to establish the new equilibrium. An undersaturated situation is created when the pressure is brought to a higher pressure and/or a lower temperature than in the initial case.

The amount of gas that the solution can absorb from or has to deposit to the surrounding environment can be characterized by the dimensionless saturation ratio ζ defined by:

$$\zeta = \frac{C_I}{C_S} - 1 \tag{2.2}$$

For an oversaturated solution $\zeta > 0$ and for an undersaturated solution $\zeta < 0$. In the initial situation the solution is fully saturated which implies $\zeta = 0$.

2.2 Experimental properties

The main mechanism that drives bubble growth or dissolution is the diffusion of gas caused by the concentration gradients which are induced when the solution becomes over- or undersaturated. With the amount of oversaturation used in our experiments, bubble growth requires the pre-existence of gas pockets (so-called nucleation sites) in the solution. We control the saturation ratio through accurate control of the pressure in the experimental chamber (see section 3.3) and use hydrophobic pits on silicon wafers to provide controlled nucleation sites (see section 3.4). The pressure profile shown in figure 2.1 will be used as guideline to explain each stage of the experiment.

In the first stage the solution is at an equilibrium saturated state where the concentration is given by $C_I = k_H P_I$. The pressure is decreased during the second stage to a pressure $P_L < P_I$. This leads to an oversaturated state where the pre-existing gas pocket in the substrate will start to grow. The pressure will stabilise in the third stage. The bubble will grow larger than the pit and the concentration at the surface of the bubble is given by $C_S = C_L = k_H P_L < C_I$ (at the same temperature T_I) neglecting Laplace pressure. The influence of surface tension is limited to the first instants of growth and the last phase of dissolution. When the bubble has grown to a certain size the pressure is raised to a higher final pressure than the initial pressure, $P_F > P_I$. In this fourth stage the solution change from over- to undersaturated and the radius will decrease fast due to the pressure change. In the last stage the final pressure is stable and the bubble will dissolve mainly due to the undersaturated situation where the concentration on the surface of the bubble is, $C_S = C_F = k_H P_F > C_I$.

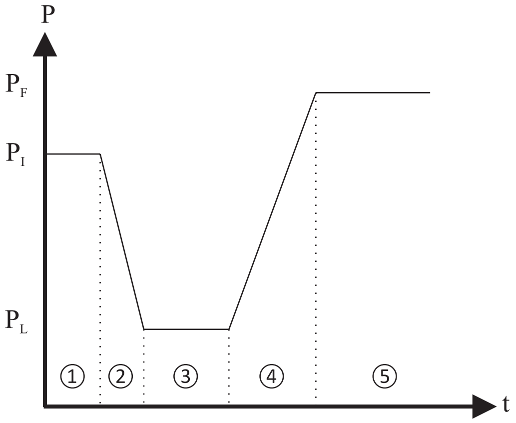

Figure 2.1: Schematic representation of the pressure over time. The 5 important stages in the pressure are given. 1) Pressure is at its initial value P_I and the solution is completely saturated. 2) The pressure decreases to create an oversaturated solution. 3) Stable pressure, lower than the initial pressure P_L. The bubble will grow during this stage due to the oversaturated conditions. 4) Pressure is raised to a higher pressure than the initial pressure denoted by the final pressure, P_F. This is a transition stage from an over- to an undersaturated solution. 5) Stable final pressure, the solution is undersaturated solution and the bubble will dissolve.

A schematic representation of the properties of the bubble is shown in figure 2.2. The bubble has a radius R and is surrounded by a concentration boundary layer with thickness $\delta = \sqrt{\pi D t}$, where D is the diffusion constant. The concentration at the surface of the bubble is given by $C_S = k_H(T_I)P(t)$, where k_H is constant the whole time because the process is done under isothermal conditions with temperature T_I. The concentration at $r = R + \delta$ and farther away is equal to the initial concentration C_I. The concentration profile will develop from C_S at $r = R$ to the concentration C_I at $r = R + \delta$ in the radial direction within the boundary layer. During the growth stage the porfile can be given by:

$$C(r) = C_S - (C_S - C_I)\frac{1 - \frac{R}{R+\delta}}{1 - \frac{R}{r}} \tag{2.3}$$

where $C_S = k_H P_L$ at that moment [25, p.45]. This is the natural profile that will develop when a solution is brought instantaneously from a saturated to an oversaturated state. For simplicity this profile is shown as linear in figure 2.3a in order to explain the evolution of the gas concentration around the bubble when the pressure is risen again. When the pressure is raised to its final pressure the concentration profile becomes more complicated because the profile from $C_L < C_I$ to C_I will partly remain over a distance between

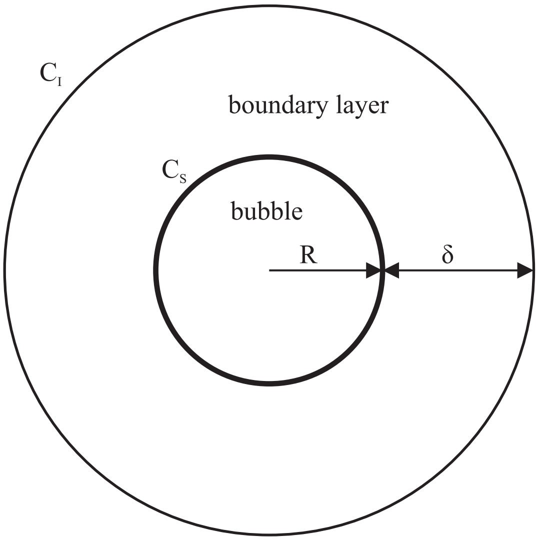

Figure 2.2: Sketch of growing/dissolving bubble. The bubble has a certain radius that develops over time, $R(t)$. Around the bubble there is a boundary layer, $\delta = \sqrt{\pi D t}$. In this boundary layer there is a concentration profile from the concentration at the surface, C_S, to the concentration of the bulk solution, C_I.

$r = R{+}L$ and $r = R{+}\delta$ and a new profile will develop from $C_F > C_I$ to C_I as shown in figure 2.3b. The bubble feels an undersaturation of $C(R{+}L)/C_F{-}1$ and therefore gas will flow from the bubble into the boundary layer. The surrounding liquid feels an oversaturation of $C_I/C(R+L)-1$ and therefore gas will flow from the solution into the boundary layer. With those inflows of gas the concentration profile will be filled up to come closer to the natural profile as given by equation 2.3 only now with $C_S = k_H P_F$. The net flow of gas will determine if the bubble dissolves or grows.

The previous examples correspond to a final undersaturated state (i.e. $P_F > P_I$). Throughout our experiments, values for the initial pressure and the low pressure were always the same. However, we investigate three different cases for the final pressure, namely: i) $P_F > P_I$ as we just described, ii) $P_F = P_I$, which means that the solution is brought back to the original saturation codition, and iii) $P_L < P_F < P_I$, where the solution is still marginally supersaturated, and which can in principle lead to a stable bubble as will be disscussed in section 5.3.

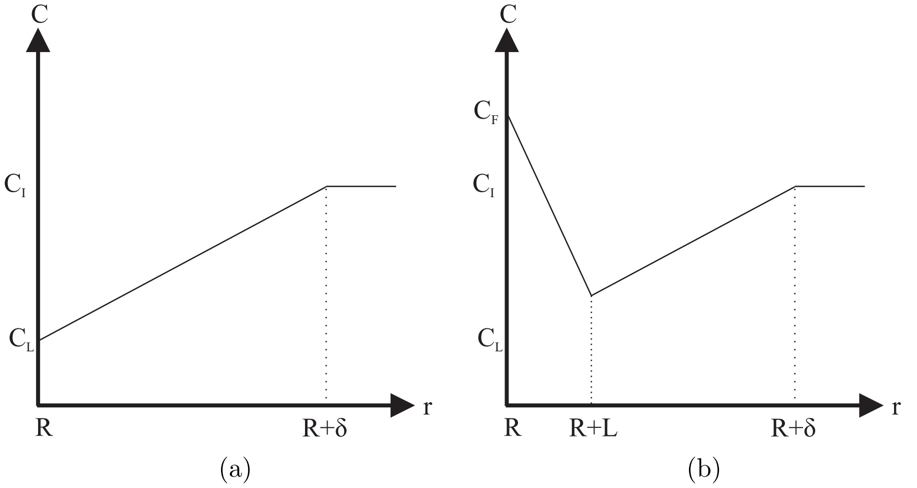

Figure 2.3: Schematic representation of the concentration profile in the radiual direction of the boundary layer at a certain time t. a) At this moment the solution is slightly oversaturated. In this situation the concentration at the bubble surface is equal to the lowest concentration $C_S = C_L = k_H P_L$. For simplicity, the concentration profile will be represented with a linear gradient between C_S at $r = R$ to C_I at $r = \delta > R$ and an uniform concentration farther away. b) The solution is changed from over- to undersaturated. The surface concentration is now equal to the final concentration, $C_S = C_F = k_H P_F$. Therefore, the boundary layer is “trapped” between two higher concentrations (C_F and C_I) and will get a gas influx both from the dissolving bubble and the surrounding liquid. The graph b) shows a simple sketch of how the concentration profile might look at one moment during its evolution.

Chapter 3

Experimental aspects

The experiments are done in a controlled experimental system that can be seen as a soda machine. In this chapter will be explained how the solution of carbon dioxide dissolved in water is prepared and transported through the system. Finally the chosen parameters for the experiments will be discussed and the experimental procedure will be explained.

3.1 Experimental Set-up

The set-up is in principle a soda machine that consists of 2 tanks as shown in figure 3.1. A large tank, with a volume of 7 litres, is used as reservoir to prepare and store the gas-liquid solution (on the right within the frame). The smaller tank, with a volume of 1.3 litre, is used as observation tank (bottom left, outside frame). In this tank the experiments for controlled bubble growth and dissolution take place. A system of steel pipes and pneumatic valves connect the tanks to each other and to the water and gas sources as well as to the drainage system of the lab. The observation tank has 3 windows at an angle of 90^o and a device for holding and positioning the substrates with nucleation sites. The window at opposite side of the sample holder is used to dry the chip with air before an experiment. The two windows that face each other are used to illuminate the tank with a light and a diffuser and visualize the experiment with a camera (Flowmaster, La Vision) with a long distance microscope objective (K2/sC, Infinity). A sketch of the whole set-up is shown in figure 3.3. The specifications of the set-up are given by Enríquez et al [26].

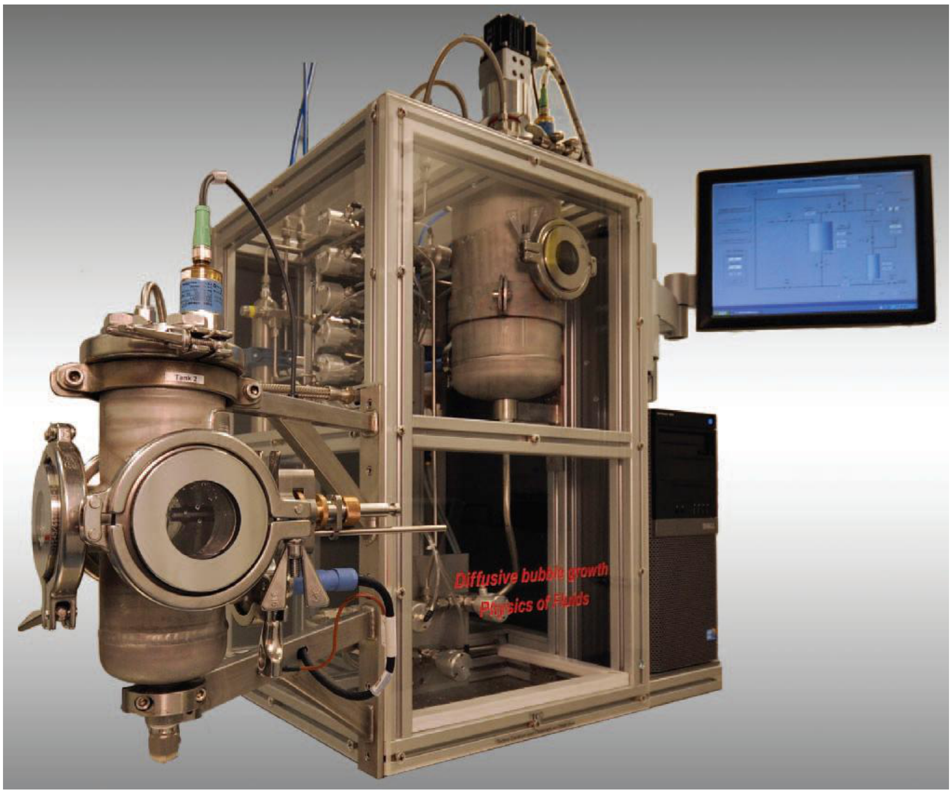

Figure 3.1: Photograph of experimental system. The observation tank is on the right-hand side in the frame. The observation tank is outside the frame in order to allow positioning of light and camera. The height of the frame is about 90 cm [26].

3.2 Reservoir tank

To prepare a solution of carbon dioxide and water the tank is first filled with ultra pure water (MiliQ A10, Millipore) to a level such that there is enough space left for a gas layer on top. Then the liquid is exposed to pressurized CO_2 (provided by Linde Gas with 99.99% purity) of 0.65 MPa. The saturation process of the solution is accelerated by a stirrer attached to a gassing propeller which is powered by a motor. Figure 3.2 shows how the mixer acceleates the saturation process. The rotation of the propeller blades create a low pressure region around them. Due to this rotation gas is sucked into the hollow stirrer axis and blown into the liquid through holes at the end of the propeller blades. With this mechanism it takes less than 45 minutes to fully saturate the solution in this tank. The solution is left overnight to allow the temperature to settle.

Before an experiment the solution is mixed for 35 minutes at a rate such that the depth of the vortex created by the stirring mechanism is approximately half of the total depth of the water volume in the tank. After this time the speed is slowed down such that the surface has a small curvature. This speed is hold for 10 minutes to ensure that the solution is not too agitated. For the last 5 minutes the CO_2 inlet is closed to be sure that the pressure that is measured inside the tank represents the pressure in the solution. The mean value of the pressure and temperature of those last 5 minutes are taken as representing parameters for the saturated solution.

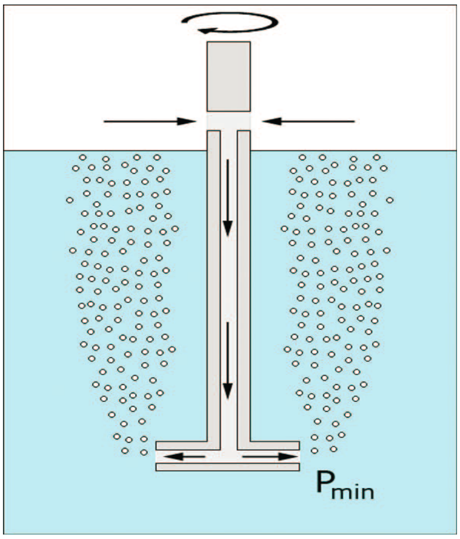

Figure 3.2: Sketch of the gassing mixer used. The rotation of the propeller blades creates low pressure zone. As a result, CO_2 is sucked into the hollow stirrer axis and bubbled into the liquid through the end of the propeller blades [26].

3.3 Observation tank

The observation tank is at the start of the procedure empty and at atmospheric pressure. Before the tank is filled with solution, the chip with artificial nucleation site is blown dry with an air gun.

Then the tank is flushed with CO_2 for 1 minute to expel atmospheric gasses. After this procedure the pressure is raised to the same value as in the reservoir tank to avoid a sudden high pressure inflow of solution. The valves between the two tanks are then opened and water flows slowly into the observation tank driven by the slightly higher position of the reservoir tank as shown in figure 3.3. A level switch ensures that the tank is always filled to the same level. After this procedure the solution is left to stabilize for 3 minutes to ensure that the solution is quiescent.

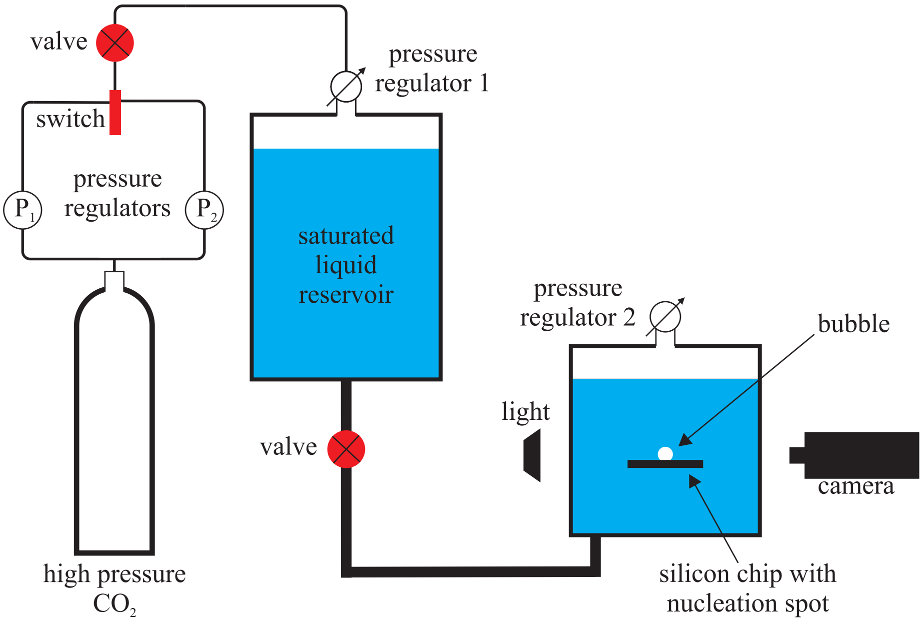

Figure 3.3: Sketch of the experimental set-up. With the pressure regulators two different pressures can be provided: one to saturate the solution and another to make the solution undersaturated. In the large thank the gas liquid solution is prepared and stored. Trough the system of steel pipes and pneumatic valves a portion of the solution can be transferred to the observation tank. There the bubble can grow on a hydrophobic micro-pit etched on a silicon chip. The temperature in the system is kept stable by circulating water from a refrigerated cooler through a hose wrapped around the tank (see [26]). The process is visualised through a window in the tank using a camera with a long-distance microscope objective with diffusive back light at the opposite window.

3.4 Experimental settings

The experiments are visualized by a camera with a long distance microscope objective. With custom made software, the images are acquired and processed. The images are saved at a frequency of 2 Hz and processed data (contour of the bubble) and the temperature and pressure of the observation tank are taken at a frequency of $\sim$ 5 Hz.

The bubbles are grown on a micro-sized pit with a radius of $R_p = 50\ \mu m$ and a depth of $\sim 30 \mu m$ etched on a rectangular silicon chip (8×30 mm). A super-hydrophobic structure is present on the bottom of the pit in order to ensure that gas will be entrapped inside the pit after being submerged in water. This size of the pit is chosen in order to have a wide range of bubble radii before the bubble detaches (maximal bubble radius before detachment is $R_{det} \approx 800\ \mu m$ [20]).

To create an experiment that is reproducible the bubbles are grown to a predefined size. To define a size, the onset time where natural convection plays a dominant role is taken into account because the growth rate will be enhanced due to natural convection [20]. For a bubble that grows after a pressure drop of 0.10 MPa from the initial pressure of 0.65 MPa this onset time is approximately 77 seconds [21, p. 49]. The sizes to which the bubbles grew are chosen such that they are below, around and above this onset time. This correspond to bubbles with a radii of 90, 150 and 310 μm.

The bubble will grow in an oversaturated environment where the pressure is reduced 0.10 MPa form the initial pressure of 0.65 MPa. The final saturation states are chosen such that the bubble will dissolve due to surface tension ($P_F = P_I$), dissolve due to undersaturated conditions ($P_F > P_I$) and to create a stable bubble ($P_F \approx P_I$). All the experiments are done with a temperature of $20.2 \pm 0.2\ ^oC$.

When the solution is stabilized in the observation tank the inflow of CO_2 is closed and the pressure switched to the other inlet if necessary. The recording of the images and data points in the observation tank are started at the same time in order to correlate the radius of the bubble with the right pressure conditions. The pressure is lowered in a controlled way to create an oversaturated condition. After this pressure drop a bubble starts to grow on the chip. When the bubble reached its defined size the CO_2 inflow is opened again. The experiment is finished when the bubble fully dissolved or the bubble started to grow after the second pressure change.

Experimental data of the pressure and radius are respectively shown in figure 3.4a and 3.4b for a final undersaturated solution.

The blue part represents the grow stage of the bubble ($\zeta \approx 0.19$), the green part dissolution mainly due to the pressure change and the red part dissolution mainly due to diffusion ($\zeta \approx -0.18$). In figure 3.5, 4 images of the lifetime of the bubble corresponding to those signals are shown.

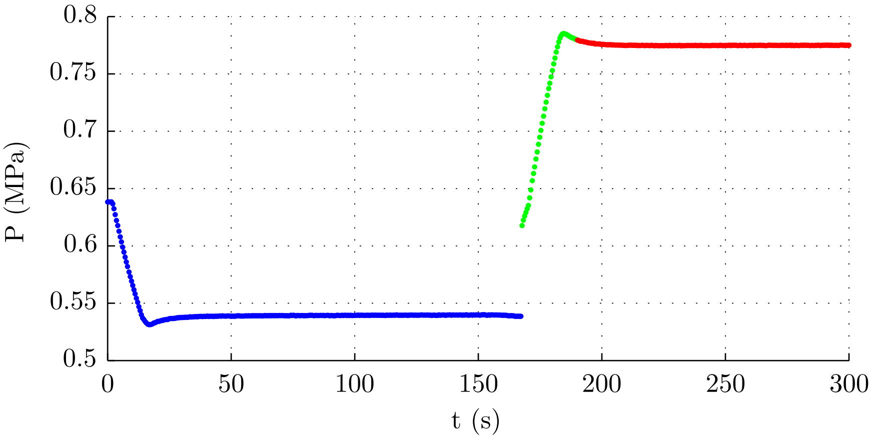

(a)

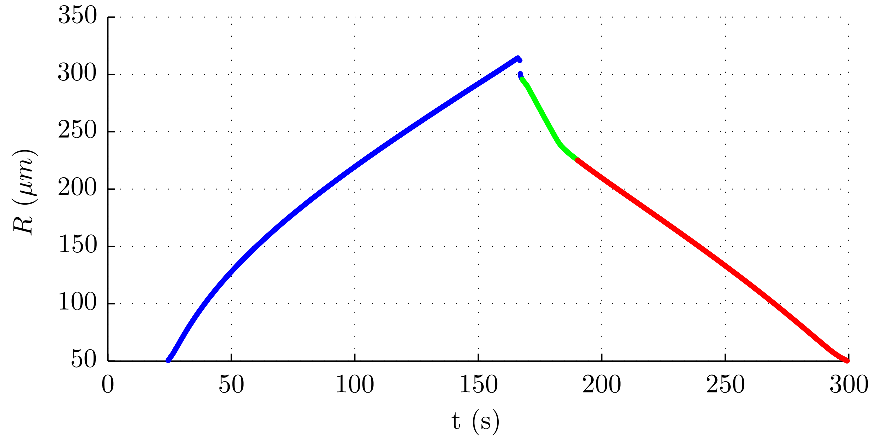

(b)

Figure 3.4: Experimental data for for the growth and dissolution of a CO_2 bubble. a) Pressure as function of time, b) Radius as function of time. The solution is saturated at an initial pressure of $P_I = 0.639$ MPa and temperature $T_I = 20.2\ ^oC$. Three stages during the process are indicated: i) Growth during oversaturated conditions of $\zeta \approx 0.19$ (blue), ii) pressure increase (green) and iii) dissolution during undersaturated conditions of $\zeta \approx -0.18$ (red).

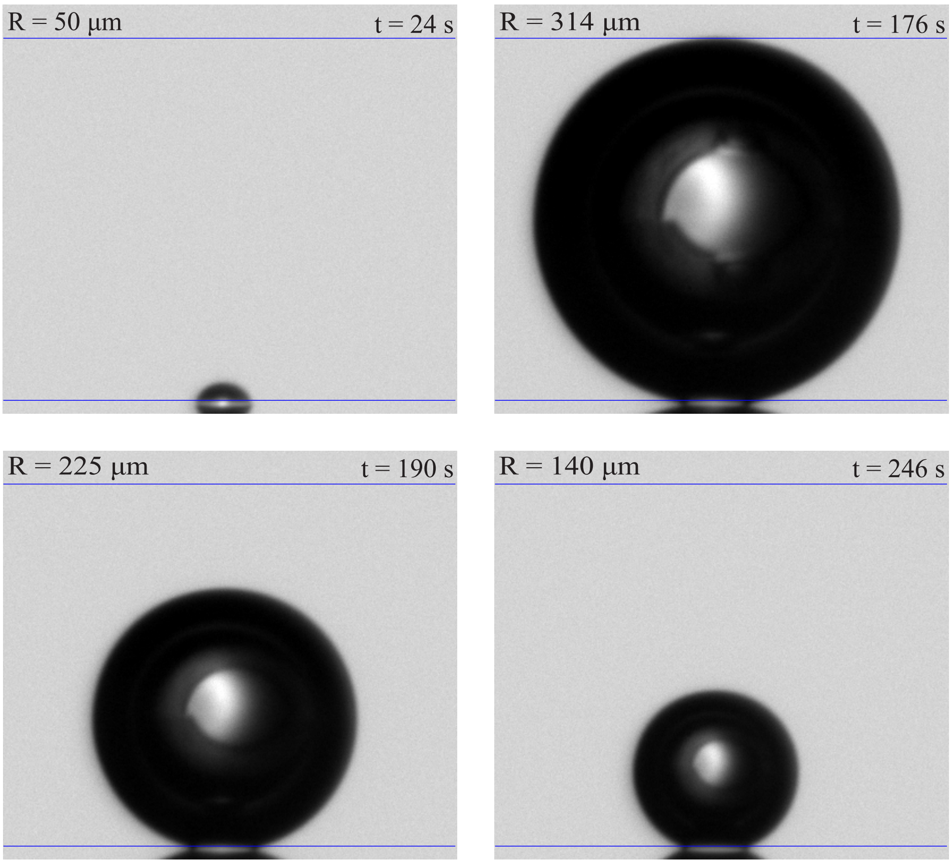

Figure 3.5: Pictures of the different stages during bubble growth and dissolution corresponding to the data in figure 3.4. Top left picture is the moment when the bubble is a hemisphere (corresponding to the first point in figure 3.4b). The top right picture is the moment where the predefined radius is reached. Bottom left picture is the first moment that the pressure reached its final value. Bottom right picture is 56 seconds after the pressure has reached its final value.

Chapter 4

Theoretical aspects

In this chapter the theoretical relation for the evolution of the radius of a gas bubble on a substrate in a gas-liquid solution with different saturation conditions will be derived. To do so, first the ideal situation as formulated by Epstein and Plesset will be explained. Then a factor will be given to determine the effective area for mass transfer. Finally we derive a "history term" to account for the effects of the concentration profile in the dissolution of the bubble. After the derivation an explanation will be given about how it is implemented in a numerical model.

4.1 Idealized situation

Epstein and Plesset define an idealized problem where a bubble grows or dissolves due to diffusion in an unbounded and isothermal respectively, over- or undersaturated gas-liquid solution. The initial equilibrium concentration of the solution is given by $C_I = k_H P_I$ at a temperature T_I (Henry's law). When the pressure is changed this leads to an out of equilibrium state that can be over- or undersaturated. At $t = 0$ a spherical bubble with an initial radius R_0 will be placed in this gas-liquid solution. The concentration on the boundary of the bubble can be given by $C_S = k_H P_S$ (at the same temperature T_I). The center of the bubble remains at the origin of a spherical coordinate system.

4.2 Pressure changes

The experimental situation differs in the fact that the pressure is not constant but changes during the experiment. To analyse only the change in radius due to diffusion the experimental data is multiplied by a factor that compensates for the pressurese changes. This factor is deduced from the ideal gas law which states: $PV = constant$. The initial pressure P_I is taken as ambient pressure in the gas-liquid solution because the liquid is saturated as this pressure. So the compensated radius will be given by;

$$R^*(t) = R(t)\sqrt[3]{\frac{P(t)}{P_I}}, \tag{4.1}$$

were $R(t)$ is the measured radius, $P(t)$ the pressure at the same time and P_I the initial pressure of the bulk of the solution.

4.3 Influence of the chip

In the ideal case the bubble grows or dissolves in an infinite medium but in the experimental case the bubble grows on a substrate. Therefore the mass transfer is reduced in the experimental case. This is caused by two effects: 1) The bubble can not be treated as spherical because it does not grow much larger than the pit radius, and 2) The chip acts like a barrier which hinders mass transfer into or out of the bubble. Those effects can qualitatively be estimated by removing the mass diffusing across the dashed area of the bubble surface shown in figure 4.1, where the larger sphere represents the edge of the boundary layer of thickness $\delta = \sqrt{\pi D t}$. With a simple geometric calculation the "effective" area can be determined that remains for mass transfer. This area is given by:

$$A_{eff} = 4\pi R^2 \left(\frac{1}{2} + \frac{1}{2}\frac{\sqrt{1 - \left(\frac{R_p}{R}\right)^2}}{1 + \frac{\delta}{R}} \right) = 4\pi R^2 f_A(t) \tag{4.2}$$

When the mass transfer at the boundary of the bubble is determined the effective area A_{eff} has to be used instead of the full bubble surface. This is the same as multiplying the equation for mass transfer by factor f_A.

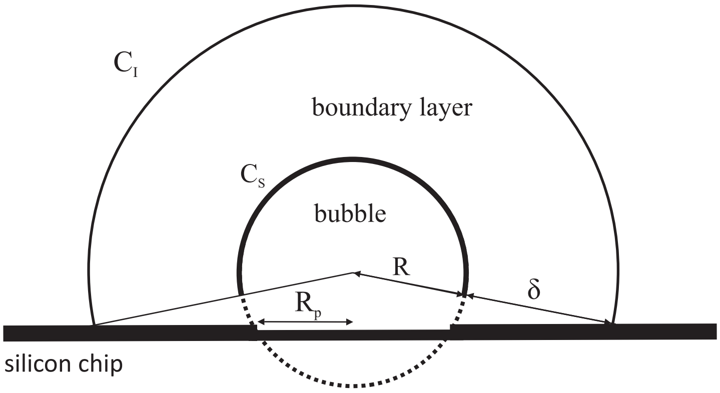

Figure 4.1: Sketch to illustrate the interaction of the boundary layer with the silicon chip and the fact that the bubble can not be treated as a sphere. The excluded bubble area (dashed line) is estimated using the cone formed by the center of the bubble and intersection of the boundary layer (shown by the bigger sphere) with the silicon chip.

4.4 Formulation of the diffusive problem

We start with the ideal situation as described by Epstein and Plesset. The gas concentration C, obeys the convection-diffusion equation,

$$\partial_t C + \dot{R}(t)\frac{R(t)^2}{r^2}\partial_r C = D\frac{1}{r^2}\partial_r(r^2\partial_r C) \tag{4.3}$$

with the boundary conditions:

$$r = R(t) \qquad : C(R(t),t) = C_S(t) + k_H\frac{2\sigma}{R} = k_H\left(P(t) + \frac{2\sigma}{R}\right) \tag{4.4}$$

$$R \to \infty \qquad : C(\infty,t) \to C_I \tag{4.5}$$

and the initial condition: $C(r,0) = C_I$. Henry's law is applied on the pressure that is present on the boundary of the bubble. This pressure consists of the gas pressure $P(t)$ and the Laplace pressure $2\sigma/R$, where $\sigma = 0.069\ N/m$ is the surface tension of the gas-liquid interface. The diffusion constant is $D = 1.97 \times 10^{-9}\ m/s^2$

By using the arguments of Epstein and Plesset [22] the convective term will be neglected. This condition is well justified when Peclet number is small $Pe = R\dot{R}/D \ll 1$. So with this assumption equation 4.3 transforms into:

$$\partial_t C = D\frac{1}{r^2}\partial_r(r^2\partial_r C) \tag{4.6}$$

The problem will made dimensionless using the following rescaled

$$\text{radial coordinate} \qquad \xi = \frac{r}{R(t)} \tag{4.7a}$$

$$\text{time change} \qquad d\tau = dt\frac{D}{R(t)^2} \tag{4.7b}$$

$$\text{concentration} \qquad c(\tau) = \frac{C(t)}{C_I} - 1 \tag{4.7c}$$

$$\text{radius} \qquad a(\tau) = \frac{R(t)}{R_I} \tag{4.7d}$$

Where R_0 is the radius at $t = 0$ this radius is not defined in the experiments so another length scale have to be defined.

When those dimensionless parameters are used to make equation 4.6 dimensionless and neglecting therms of order $O(Pe)$ (see appendix A), the problem could be written as:

$$\partial_\tau c = \frac{1}{\xi^2}\partial_\xi(\xi^2\partial_\xi c) \tag{4.8}$$

with the boundary conditions:

$$\begin{aligned} \xi = 1 \qquad &: c(1,\tau) = \bar{c}_S(\tau) \qquad &&= \frac{C_S + k_H\frac{2\sigma}{R}}{C_I} - 1 \\ & &&= c_S(\tau) + \frac{k_H}{C_I}\frac{2\sigma}{a(\tau)R_0} \\ & &&= c_S(\tau) + \frac{\eta}{a(\tau)R_0} \qquad (4.9) \\ \xi \to \infty \qquad &: c(\infty, t) \to 0 && \qquad (4.10) \end{aligned}$$

and the initial condition $c(\xi, 0) = 0$. For brevity in the above and further expressions we use $c_S = C_S/C_I - 1$ and $\eta = 2\sigma k_H/C_I$.

The solution will be sought in the form $c(\xi,\tau) = f(\xi,\tau)/\xi$. From equation 4.8 this function, f, satisfies:

$$\partial\tau f = \partial_{\xi\xi} f \tag{4.11}$$

With this equation we want to obtain an expression for the mass flow across the bubble surface ($\zeta = 1$). To do so the Laplace transform of equation 4.11 is taken. Taking into account the initial condition $f(\xi, 0) = 0$ gives the differential equation:

$$s\hat{f} = \frac{d^2\hat{f}}{d\xi^2} \tag{4.12}$$

This equation can be solved in combination with boundary conditions 4.9 and 4.10, which gives the following solution:

$$\hat{f}(\xi, s) = \hat{\bar{c}}_S e^{-\sqrt{s}(\xi-1)} \tag{4.13}$$

To compute the mass flux across the bubble surface ($\xi = 1$), it suffices to evaluate:

$$\partial_\xi \hat{c}|_{\xi=1} = \hat{f}'(1,s) - \hat{f}(1,s) = -\sqrt{s}\hat{\bar{c}}_S - \hat{\bar{c}}_S \tag{4.14}$$

This expression can be transformed back to the time domain using the convolution theorem:

$$\partial_\xi c|_{\xi=1} = -\mathcal{L}^{-1}\left[\frac{1}{\sqrt{s}} s\hat{\bar{c}}_S\right] - \bar{c}_S = -\int_0^\tau \frac{1}{\sqrt{\pi(\tau-\tau')}}\frac{d\bar{c}_S}{d\tau'}d\tau' + \bar{c}_S \tag{4.15}$$

The part within the integral describes the influence of the concentration in the boundary layer on the flux across the bubble surface and is therefore called the history term. The other term is the flux induced by the relative difference in concentration between the concentration on the bubble surface and the concentration of the bulk solution. In the history term is used c_S is used instead of $\bar{c}_S = c_S + \frac{\eta}{aR_0}$. This replacement can be done because $d\bar{c}_S/d\tau \approx dc_S/d\tau$ for bubbles of micrometer scale.

4.5 Epstein-Plesset equation with history term

A similar expression to the Epstein-Plesset equation will be derived for the real situation (including the influence of the chip) from the equation for mass conservation. Laplace pressure is taken into account in this derivation and the gas inside the bubble is treated as ideal,

$$\frac{dm}{dt} = \frac{d}{dt}\left(\frac{4}{3}\pi R(t)^3\rho(t)\right) = 4\pi R^2 D f_A(t)\partial_r C|_{r=R} \tag{4.16}$$

where $\rho(R(t))$ is the gas density inside the bubble. This density will be deduced from the ideal gas law and in combination with the assumption that the process is isothermal the relation becomes:

$$\frac{M}{k_H BT}\left(\frac{R}{3}\dot{C}_S + C_S\dot{R} + \frac{4}{3}\sigma k_H\frac{\dot{R}}{R}\right) = D f_A(t)\partial_r C|_{r=R}, \tag{4.17}$$

where M is the molar mass of CO_2 and B the ideal gas constant. The dimensionless parameters as defined in 4.7 are used to make the above equation dimensionless. An equivalent to the Epstein-Plesset equation in dimensionless form is then given by:

$$\frac{da}{d\tau} = -\frac{a}{(c_S+1)+\frac{2}{3}\frac{\eta}{aR_0}}\left\{\Lambda f_A(\tau)\left[\int_0^\tau \frac{1}{\sqrt{\pi(\tau-\tau')}}\frac{d\bar{c}_S}{d\tau'}d\tau' + \bar{c}_S\right] + \frac{1}{3}\frac{dc_S}{d\tau}\right\} \tag{4.18}$$

where $\Lambda = k_H BT/M$ and the area correction factor for the effective area is given by:

$$f_A(\tau) = \frac{1}{2} + \frac{1}{2}\frac{\sqrt{1-\left(\frac{Rp}{a(\tau)R_0}\right)^2}}{1+\sqrt{\pi\tau}}, \tag{4.19}$$

with R_p the radius of the pit.

The $da/d\tau$ of equation 4.18 is given by 3 components:

history effects $$-\frac{a}{(c_S+1)+\frac{2}{3}\frac{\eta}{aR_0}}\Lambda f_A(\tau)\int_0^\tau \frac{1}{\sqrt{\pi(\tau-\tau')}}\frac{d\bar{c}_S}{d\tau'} \tag{4.20a}$$

concentration $$-\frac{a}{(c_S+1)+\frac{2}{3}\frac{\eta}{aR_0}}\Lambda f_A \bar{c}_S \tag{4.20b}$$

concentration difference $$-\frac{a}{(c_S+1)+\frac{2}{3}\frac{\eta}{aR_0}}\frac{1}{3}\frac{dc_S}{d\tau} \tag{4.20c}$$

Equation 4.20a is called the history term because the influence of the concentration profile in the boundary layer is taken into account. The second component (equation 4.20b) describes the contribution due to the relative difference in concentration at the surface of the bubble and in the bulk of the solution. The third component describes the contribution of the relative change of the concentration in time at the bubble surface.

4.6 Numerical simulations

The integral equation derived in the previous subsection (equation 4.18), will be used in an algorithm with the appropriate boundary conditions to simulate the theory. The integral will be evaluated using the algorithm suggested by Elghobashi et al. [27] for the Basset force in the motion of solid particles through a liquid. The solution of those simulations will be compared with the experimental results.

The experiments are comparable from the moment that the size of the bubble is such that it is equal to a hemisphere with radius $R^* = 50\ \mu m$. Therefore the scaling radius is chosen to be $R_0 = 50\ \mu m$.

As can be seen figure 3.4 the bubble reades a radius of 50 μm after the pressure is dropped to its lowest value. However the simulation needs a double pressure drop to represent the theory. Therefore a pressure drop of 0.10 MPa is used that has approximately the same dimensions as in the experiments as shown in figure 4.2a. The experimental pressure $P(t)$ is used to compute a representative pressure profile $p(\tau)$ for the simulations from the moment the pressure starts to rise. The experimental radius $R^*(t)$ had to be used to obtain the right conversion from $t \rightarrow \tau$ because the dimensionless time increase is given by 4.7b. In figure 4.2b is shown the comparison of the experimental and numerical data for the pressure increase where the latter has been converted back from τ to t. A small difference can be observed between the two graphs, which is likely to be caused by the conversion $t \leftrightarrow \tau$. The dimensionless radius $a(\tau)$ is multiplied by $R_0 p(\tau)/p(0)$ to compensate for the pressure changes and the signal is then transformed back to the time domain such that it can be compared with the experimental radius. The time between the two pressure changes (in the numerics) is adjusted such that the maximal radii of the experiments and numerical solution happen at the same point in the t-domain. The maximal radius has been chosen as the starting point for the comparison between the simulations and the experiments because the initial radius and the exact time when the bubble starts growing in experiments cannot be precisely determined due to the fact that the bubble initially grows inside the pit. This will lead to a mismatch in the boundary layer size of around 20% (for the case shown in figure 4.2) which might be one of the reasons behind the differences between experimental and numerical results.

The radius as function of time is shown in figure 4.3a for the experimental and numerical data . From this figure is clear that the growth in the numerical case takes a bit longer than in the experimental case (from the moment $R^* = 50\ \mu m$) but is of the same order. The differences may be caused by the initial conditions that are chosen. In this research the focus was on the dissolution process after the bubble has grown in an oversaturated solution. Therefore graphs are shifted such that $t = 0$ represents the moment that the pressure starts to increase because that is the moment that the radius has reached its maximum value. An illustration of this is given in figure 4.3b.

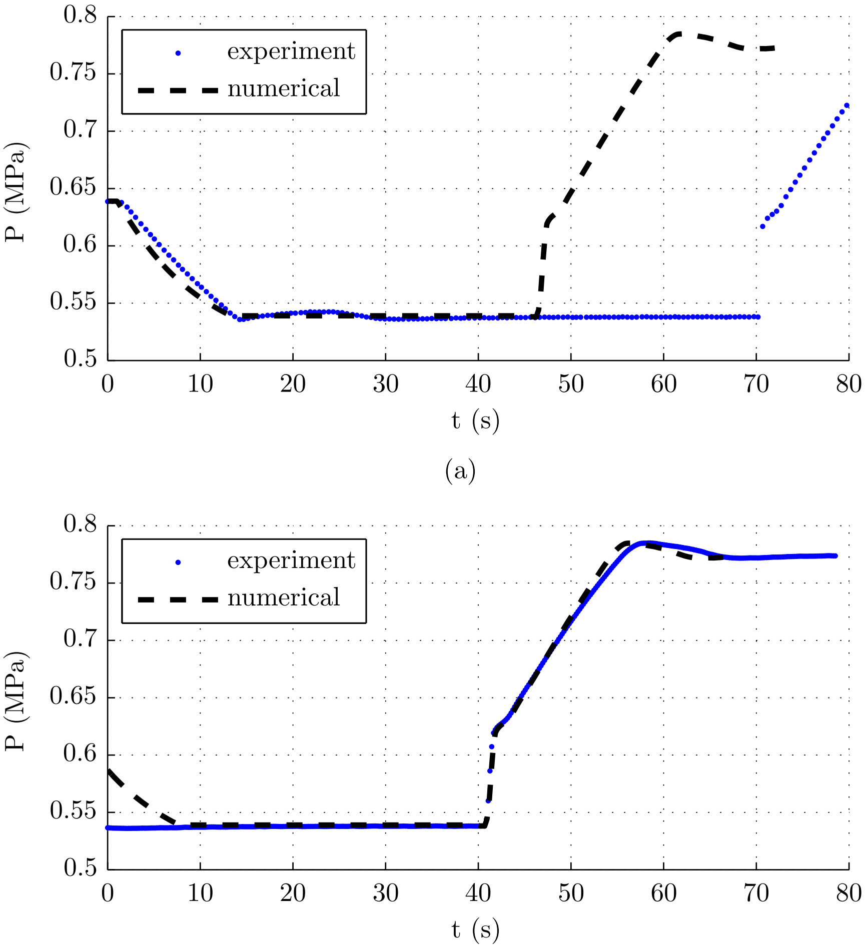

(a)

(b)

Figure 4.2: Experimental and numerical data for the pressure as function of time. a) $t = 0$ is equal to the moment that the experimental pressure decreases. The numerical pressure is adjusted such that the time to decreases is approximately the same. b) $t = 0$ is equal to the moment where $R^* = 50\ \mu m$. The numerical and experimental profiles are placed on top of each other to show that the pressure increase is approximately the same.

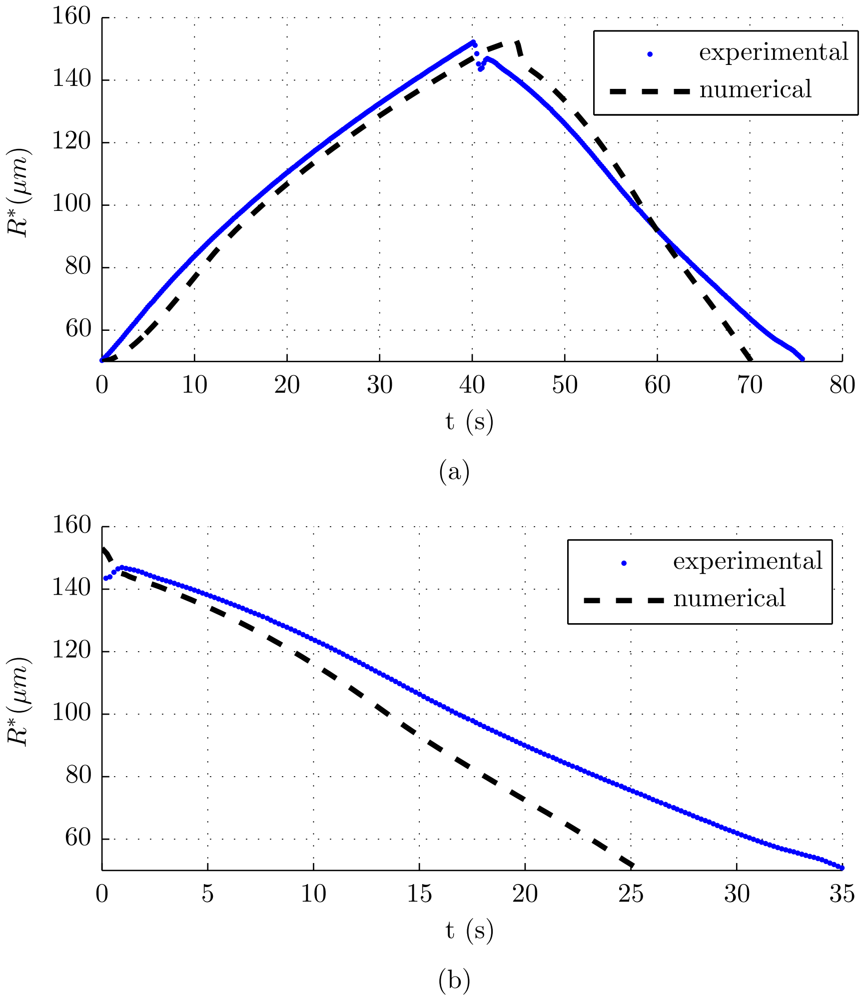

(a)

(b)

Figure 4.3: Experimental and numerical data for the radius as function of time. a) $t = 0$ correspond to the moment where $R^* = 50\ \mu m$. The pressure profile is adjusted such that the maximal radii are approximately the same. b) $t = 0$ correspond to the moment where R^* is maximal. This representation provides the best insight in the dissolution process.

Chapter 5

Results

In this chapter the results of the experiments are discussed and compared to the corresponding numerical simulations. In the first section dissolution under final undersaturated conditions will be treated. Here, the influence of convection on the dissolution process becomes visible. It is followed by a section where the final conditions are saturated. In the final section it will be addressed how a stable bubble can be produced.

5.1 Bubble behaviour in an undersaturated solution

In this section experimental and numerical results are shown for bubbles that dissolve under different final undersaturated conditions (i.e. $\zeta < 0$). The bubbles where grown at slightly oversaturated conditions of $\zeta \approx 1.18$ at a temperature of 20.1 ^oC. The bubbles were grown to a medium ($R^* \approx 150\ \mu m$) and large size ($R^* \approx 310\ \mu m$) and dissolved at final saturation values of $\zeta \approx -0.09; -0.18; -0.30$.

The results of for medium sized bubble are shown in figure 5.1. From the radius versus time profile (figure 5.1b) it is clear that the bubble in the numerical realization dissolves faster than in the experimental case. The expectation was that the dissolution time for the numerical and experimental case would be more equivalent because the undersaturated concentration differences are expected to be dominant over the influence of surface tension and the concentration in the boundary layer should evolve faster to its natural profile.

In figure 5.3a and 5.3b we show the components that contribute to the change in radius over time as given by equations 4.20a-c with the total sum for the bubble that dissolves at a final undersaturation of $\zeta \approx -0.18$. The components are calculated with dimensionless parameters and transformed from $\tau \rightarrow t$ using equations 4.7b and d. In this case the concentration difference (equation 4.20c) has a major influence on the dissolution process in the time frame when the pressure raise ($t \approx 0-30$ seconds). The concentration change over time also has influence on the history term (equation 4.20a) due to the integration over this derivative of the concentration over the total elapsed time. The contributions of the concentration differences (equation 4.20b) and the history term are in the same order during $t \approx 12-22$. Thereafter the change in radius is dominated by the concentration differences, as expected. From the same figures it becomes clear that the experimental results are between the contribution of the history effects and the total sum of the components. This could be caused by the fact that in the experimental case the boundary layer is larger and therefore the influence of the history effects is smaller.

The large bubble has a growth time that sure passes the time where natural convection becomes dominant ($t_{grow} > 77$ seconds). Therefore the mass flow is larger during the growth stage than without this dominant term. Natural convection is not included in the simulations and therefore the growth time in the simulations has to be extended more than in the other cases. In figure 5.2 the pressure and radius data are given for the three different final saturation conditions. The differences in the numerical and experimental dissolution times are relatively larger compared to the results of the medium bubble. This larger difference can be explained with the parts that contribute to the radial change in time that is shown in figure 5.3b and the description of the concentration profile in the boundary layer given in the second chapter. When the process is dominated by diffusion the concentration profile in the boundary can be represented in a simplified manner by the profile shown in figure 2.3b. In this case the bubble feels a locally undersaturated condition that is larger than the final new equilibrium undersaturation. The net mass flow from the bubble to the surroundings will therefore be larger until an natural profile has established. This concentration profile is disturbed when convection becomes dominant and therefore the effect of the locally undersaturation within the boundary layer will be diminished. This means that the mass flow from the bubble to the surroundings will be smaller. This effect is visible in the results because in the numerical simulations the concentration profile is intact (no convection included) and this bubble dissolves faster than the experiments. In figure 5.3b is also visible that the contribution of the history term has influence over a long time frame (~ 50 seconds) before the concentration difference ($\bar{c}_S$) is dominant in the radial change. This would not be the case if the boundary layer was mixed due to convection and the radial change over time would be smaller.

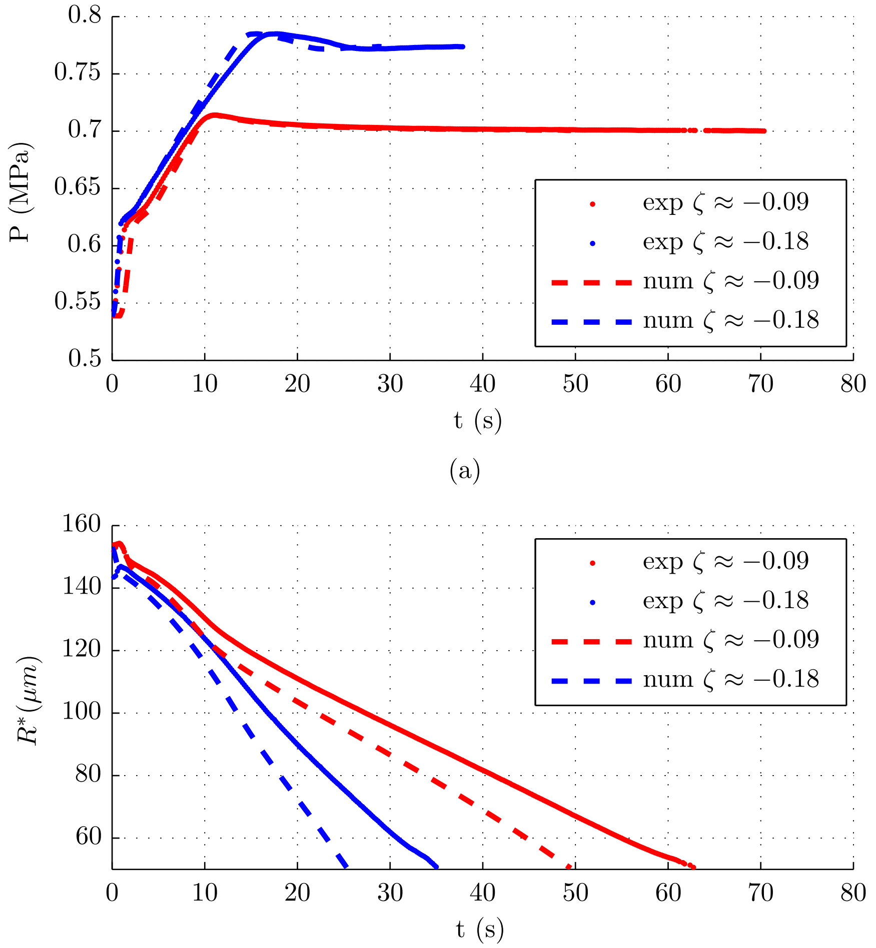

(a)

(b)

Figure 5.1: Experimental and numerical data for two different final saturation values. For both cases the bubbles grew to approximately 155 μm prior to dissolution. The red data sets are for a final saturation of $\zeta \approx -0.09$ and the blue for $\zeta \approx -0.18$. All bubbles grew at a saturation value $\zeta \approx 0.18$, with a initial pressure of 0.639 MPa and a temperature of 20.1 ^oC. a) Pressure as function of time. b) Radius as function of time.

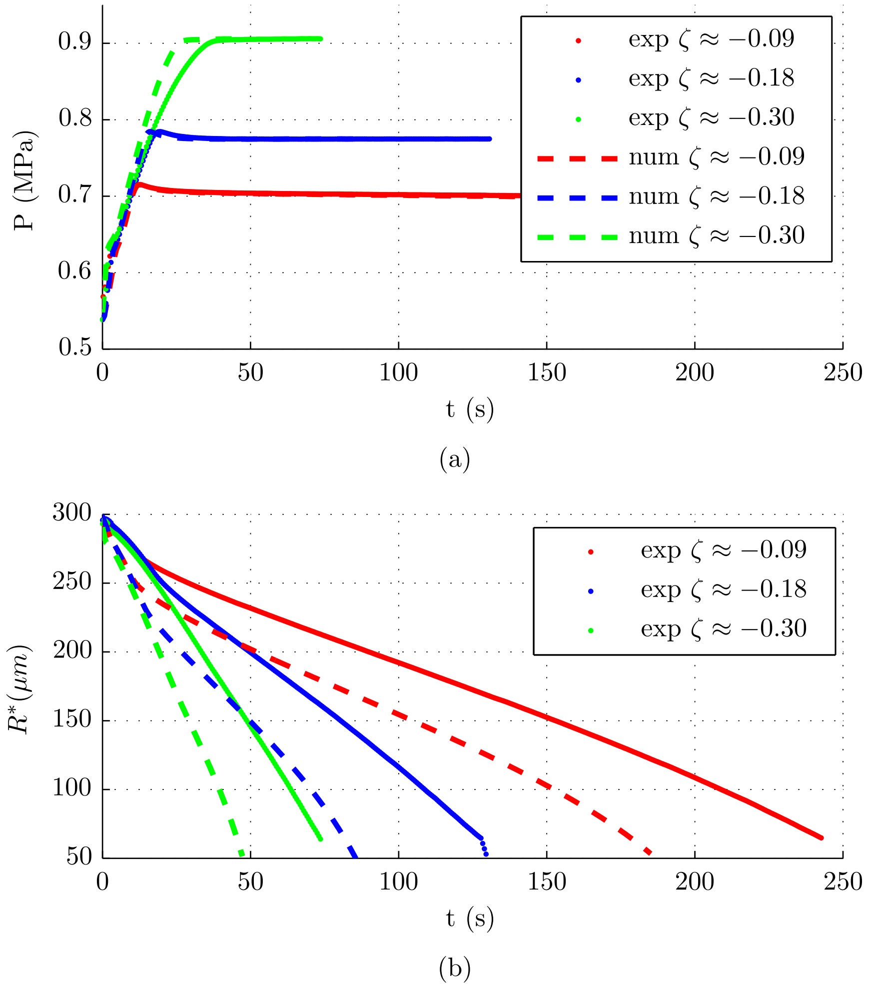

Figure 5.2: Experimental and numerical data for two different final saturation values. For both cases the bubbles grew to approximately 300 μm prior to dissolution. The red data sets are for a final saturation of $\zeta \approx -0.09$, the blue for $\zeta \approx -0.18$ and the green for $\zeta \approx -0.30$. All bubbles grew at a saturation value $\zeta \approx 0.18$, with a initial pressure of 0.639 MPa and a temperature of 20.1 ^oC. a) Pressure as function of time. b) Radius as function of time.

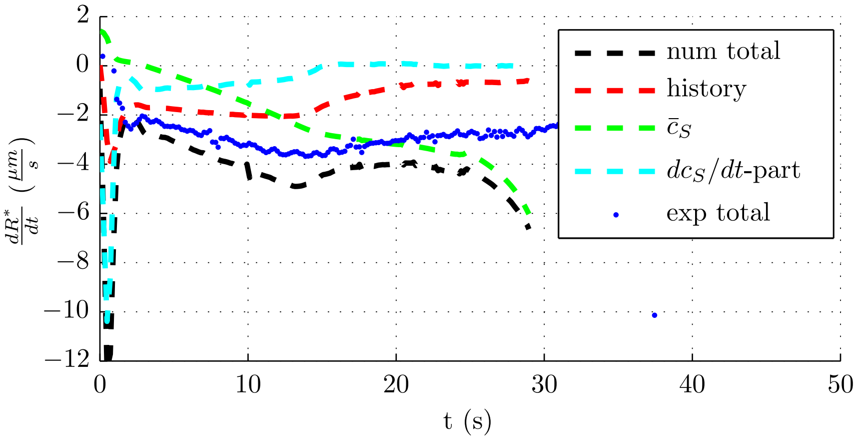

(a)

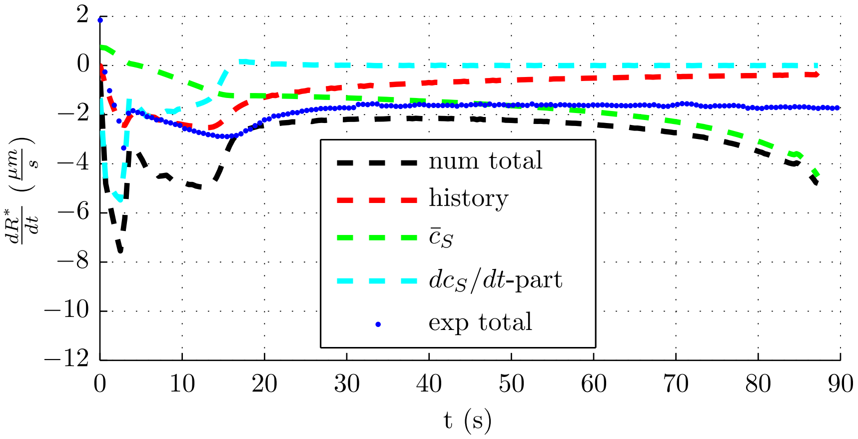

(b)

Figure 5.3: Components of the derivative (given by equation 4.20) of the radius as function of time from the numerical simulation combined with experimental results for a bubble that grow at $\zeta \approx 0.18$ and dissolved at a final $\zeta \approx -0.18$. a) Results for bubble with a medium size and b) large size. The first negative peak in both graphs is caused by the inital pressure jump from the lowest pressure to approximately the initial pressure. The decreasing ratio after this peak is caused by the overshoot of the pressure regulator.

5.2 Bubble behaviour in a saturated solution

In this section experimental and numerical results are shown for bubbles that dissolves under conditions that are close to complete saturation ($\zeta \approx 0.005$). The bubbles where initially grown at oversaturated conditions of $\zeta \approx 0.18$ at a temperature of 20.2 ^oC to radii $R^* \approx 100\ \mu m$ and $R^* \approx 160\ \mu m$ which are respectively called a small and a medium sized bubble. The marginally oversaturated conditions of the experiments ($\zeta \approx 0.005$) could not be used in the numerical simulation because the bubble would eventually start to grow. Therefore the initial (saturation) pressure in the numerical case is chosen such that the solution becomes completely saturated (i.e. $\zeta = 0$) at a constant temperature of 20.2 ^oC.

The radius as function of time for both sizes are shown in figure 5.4b. In this figure can be seen that the numerical solution needs longer to dissolve than in the experiments. In the same figure it is also visible that the bubbles still grow when the pressure is raised what was not observed during the experiments discussed in the previous section.

The growth of the bubble after the pressure starts to increase is caused by the long duration of this increase, as can be seen in figure 5.4a. In figure 5.5 all the components that contribute to dR^*/dt are shown. The concentration component (equation 4.20b) is positive during the pressure increase because the solution is still oversaturated ($-0.18 < \zeta < 0$). The concentration profile in the boundary layer also changes slowly and at a certain moment the mass flux caused by this profile changes form into to out of the bubble as can be seen by the history term (equation 4.20a). The sum of all three components causes that the bubble start to dissolve approximately 30 seconds after the pressure started to increase. This behaviour is visible in the experimental and numerical data of radius versus time as shown in figure 5.6 where the different pressure regions are indicated.

The numerical radius has a size of 154 μm when the pressure reached its stable value. The dissolution of a bubble of this size in the ideal case as Epstein and Plesset described it is approximately 3000 seconds. The substrate has a large influence slowing down the mass transfer. When correcting this dissolution time with a maximal area factor of 0.686 [28], the dissolution time becomes approximately 4400 seconds. This time is in good agreement with the numerical dissolution time.

The main difference between dissolution of the ideal case and this case is that there is a pre-existing concentration profile present at the moment the bubble starts to dissolve. The components of dR^*/dt after the pressure reached its stable value are shown in figure 5.5b. In this figure is visible that the history term (equation 4.20a) has a large influence on the total change in radius from 100 till 200 seconds. The concentration component (equation

4.20b) is dominant after 500 seconds. This is caused by the fact that the bulk concentration with respect to the bubble surface concentration due to the gas pressure inside the bubble is zero (i.e. $c_S = 0$ and $dc_S/dt = 0$). This means that a equilibrium concentration profile will establish in the boundary layer (i.e. history term $\rightarrow 0$) and the concentration difference is given by surface tension (i.e. $\bar{c}_S = \eta/(aR_0)$).

The history term plays a role in the dissolution process but it does not explain the large differences. The numerical model is very sensitive for concentration changes (i.e. pressure and temperature changes) so for a better comparison those changes have to be taken into account during the whole simulation.

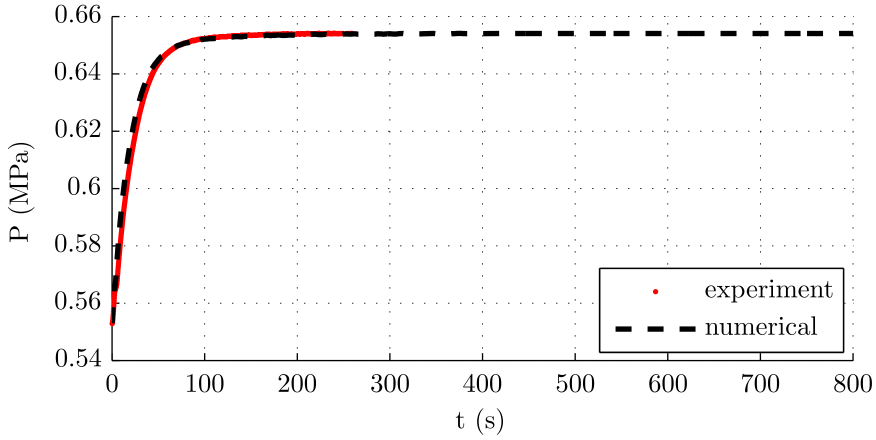

(a)

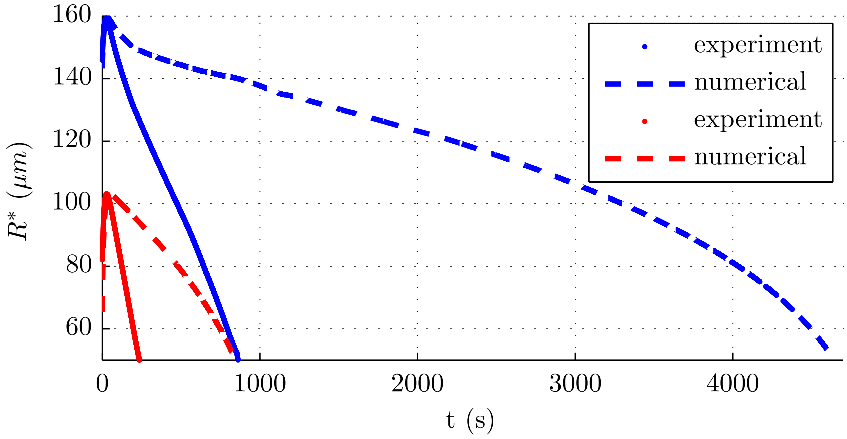

(b)

Figure 5.4: a) pressure as function of time for experimental and numerical case. b) radius as function of time for two experiments where the bubble grew to approximately $R^* \approx 160$ μm (red) and $R^* \approx 100$ μm (blue). The final saturation value in the experimental cases was $\zeta = 0.005$. The experiments are compared with numerical simulation where the final saturation was $\zeta = 0.000$. The bubbles grew at oversaturated conditions with $\zeta \approx 0.180$ with a temperature of $T = 20.2$ ^oC

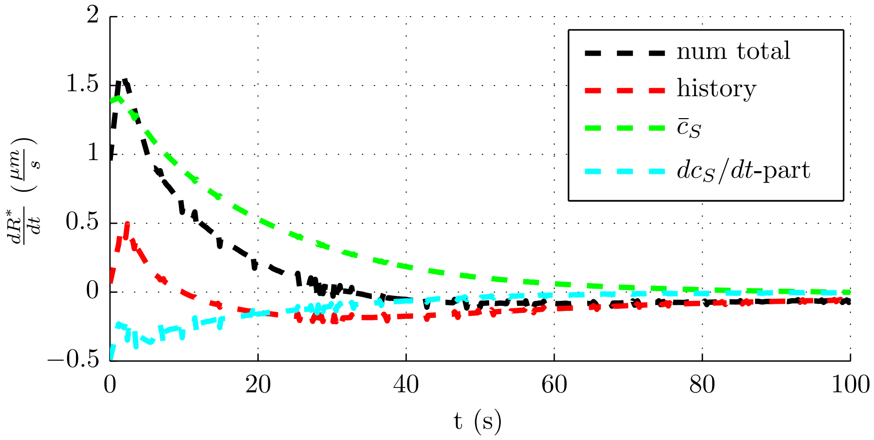

(a)

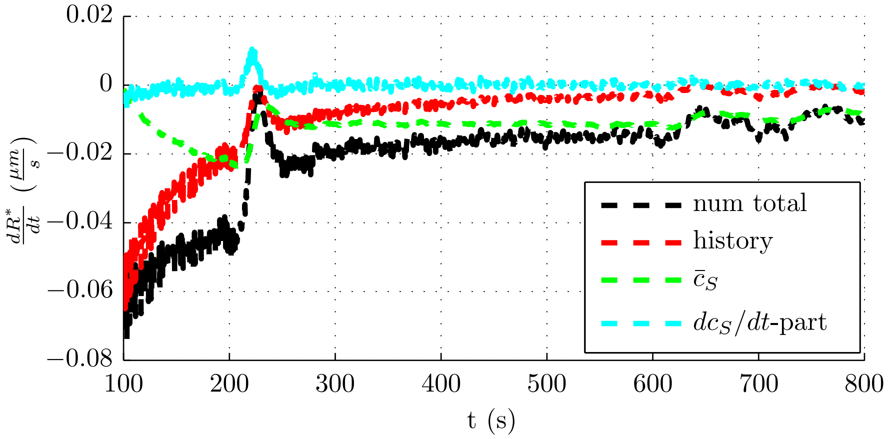

(b)

Figure 5.5: The different contributions to the derivative of the radius in time for the medium bubble under saturated final conditions. The components correspond with equations 4.20a-c). a) for the first 100 seconds. b) from 100 till 800 seconds. During pressure raise all components give a contribution. The first 100 seconds when the pressure is stable the history term is dominant. After a wile the history term tend to zero and $\bar{c}_S$ (which represents the surface tension in this case) becomes dominant. The peaks around 2 is caused by the fact that the numerical and experimental pressure profile are combined when the pressure starts to rise and the peak around 230 is caused by a small compensation due to the pressure regulator in the system.

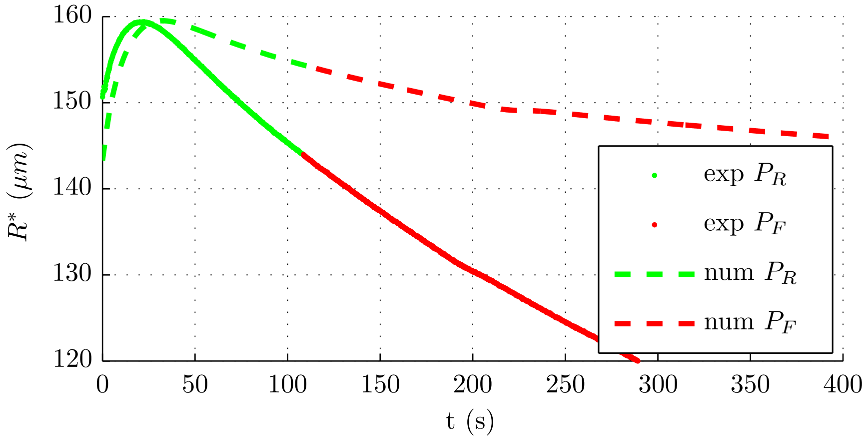

Figure 5.6: Experimental and numerical data for a medium sized bubble $R \approx 160$ μm for radius versus time. Two regions are indicated: green) pressure increase red) stable final pressure (where $\zeta = 0.005$ in for the experiments and $\zeta = 0.000$ for the numerical calculations)

5.3 Bubble behaviour in a marginally oversaturated solution

The most challenging task is to try to stabilize a bubble. In the ideal case the saturation has to be such that it compensates the Laplace pressure present due to the surface tension between the gas air interface. This pressure is for a bubble of 90 μm only 1.52 kPa which is below the precision of the pressure regulators of the experimental set-up.

From the experiments described in the previous sections it could be concluded that the applied conditions also have to compensate for the history term in the boundary layer. Therefore experiments were done where the final and initial pressure differ only 10 kPa or less. The pressure raise was made faster (about 3 seconds) to ensure that the bubble dissolve a bit during the pressure raise. The experimental results are shown in figure 5.7 for the dissolution of a small bubble that grew under oversaturated conditions of $\zeta \approx 0.19$ with a initial pressure of 0.636 MPa and a temperature of 21.4 ^oC. The final saturation values of those experiments are marginally oversaturated $\zeta = 0.01342$ and $\zeta = 0.00198$. The differences between the final pressure of those two experiments is only 5 kPa and it gave a totally different result.

Numerical calculations are made with the same initial and growth conditions as in the experiments. The final pressure is adjusted such that a stable bubble is created as can be seen in figure 5.8. The fast pressure raise induce a large change in the concentration profile of the boundary layer. Therefore the history term (equation 4.20a that describe the effects due to those changes) is dominant for the bubble behaviour for the first 3 to 10 minutes. After that moment there is still a sensitive balance between the history term and the concentration component (equation 4.20b). The numerical calculation made with saturation value of $\zeta = 0.0027939$ has the most stable results. The difference between the initial and final pressure is in this case 1.77 kPa. This is close to the Laplace pressure of a bubble with a radius of 76 μm which is 1.80 kPa, which illustrates the marginally small pressure differences that have to be compensated. The experimental equipment would have to be more sensitive and the pressure would have to be adjustable during the stabilization process to compensate for those history effects.

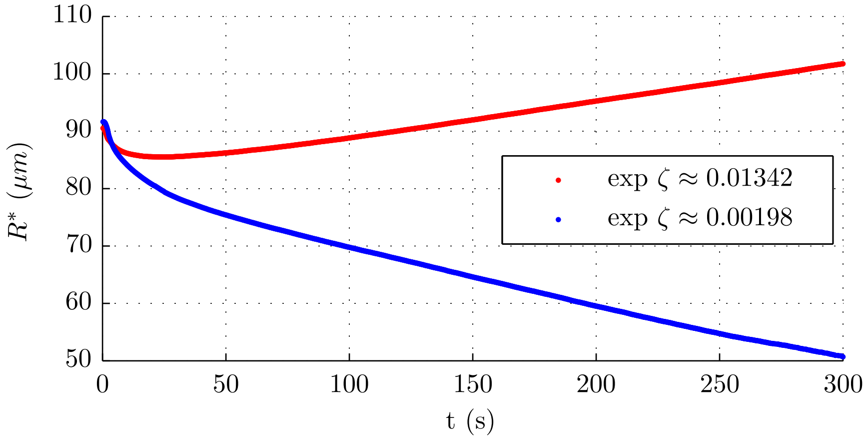

Figure 5.7: Radius as function of time for two different final saturation values as shown in the legend. The bubble that dissolves (red) had the smallest final oversaturation. This means the netto mass flow is out of the bubble. The bubble that grows (blue) does this with a smaller slope than in in the initial grow phase of the bubble. The difference between the final pressure of those two experiments is approximately 0.005 MPa for the same initial pressure of 0.636 MPa and temperature of 21.4 ^oC.

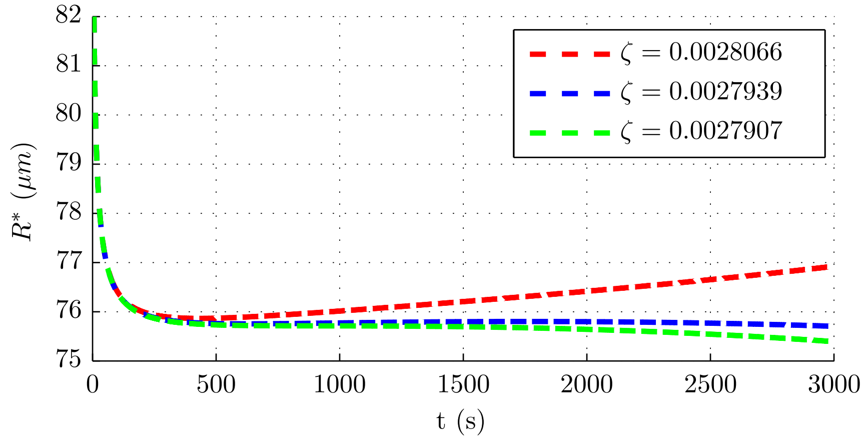

Figure 5.8: Numerical results of the radius as function of time. All bubbles grew under a oversaturation of $\zeta \approx 1.19$ (where $P_I = .636\ MPa$ and $T = 21.4\ ^oC$). The 3 different saturation values are shown the legend where the saturation pressure of the red and green curve differ only 10 Pa. Till approximately 180 seconds the curves follow the same trajectory. The blue curve is the most stable one. It has its first minimum around 10 minutes, in the next 28 minutes it grow some hundreds of nanometres and after that the bubble start to dissolve slowly.

Chapter 6

Discussion and Conclusion

The goal of this research was to investigate the dissolution process of a CO_2 bubble that dissolved conditions of saturation after it first was grown in a slightly oversaturated environment.

This process was only described by Epstein and Plesset for an ideal situation where a pre-existing gas bubble dissolved in an infinite gas-liquid solution with a certain constant saturation value. A new relation, that is comparable with the combination of Epstein and Plesset equations for growth and dissolution, was derived that could describe the process with the conditions used during the experiments.

First, experiments where carried out with under saturated condition. The numerical simulation predicted that the bubble should now dissolve mainly due to surface tension. In the experiment the bubble dissolved faster than the theory and in addition we found that the reproducibility of the experiments was quite bad.

The second series of experiments that where carried out with various undersaturated conditions were reproducible. The numerical dissolution time was in the same order but slightly faster than the experimental results. The ratio of the experimental and numerical dissolution time became higher for a bubble that grew partly dominated by natural convection compared to a bubble that grew mainly due to diffusion. This indicates that for both situations convection may play a role in the dissolution process.

Finally, experiments with a final marginally oversaturation were carried out to investigate if it was possible to create a stable bubble. From the experimental results and numerical simulation it became clear that the final pressure should be varied in a sensitive way to compensate for the Laplace pressure and history effects.

For the numerical simulation of the theory several parameters had to be chosen or estimated (scaling radius, surface tension, initial pressure drop). The simulations where done under such conditions that mimic the reality the best. Especially for bubble behaviour under saturated conditions we saw that it was sensitive to small concentration differences. More research have to be done to know if the assumption of a constant temperature can be justified.

In further research convection should be included in the derivation of the theoretical equation and there have to be checked if the assumption of a constant temperature can be justified (even tough the changes are small). The experiments could be carried out at a smaller scale to have a larger influence of surface tension and the experimental set-up can be improved with a device to regulate the pressure during the experiment.

Appendix A

Full dimensionless convection-diffusion equation

In this appendix the full dimensionless equation will be derived for the rescaled gas concentration, $c(\zeta, \tau)$ without the assuming $Pe \ll 1$. The terms of equation 4.3 becomes are stated below when the dimensionless parameters from equation 4.7.

$$\partial_t c = \partial_t \tau \partial_\tau c = \frac{D}{R_0^2} \frac{1}{a^2} \left(\partial_r c - \frac{a'}{a} \xi \partial_\xi c \right) \tag{A.1}$$

$$\dot{R} \frac{R^2}{r^2} \partial_r c = \frac{D}{R_0^2} \frac{1}{a^2} \frac{a'}{a} \frac{\partial_\xi c}{\xi^2} \tag{A.2}$$

$$\begin{aligned} \frac{D}{r^2} \partial_r \left(r^2 \partial_r c \right) &= \frac{D}{\xi^2 a^2 R_0^2} \partial_r \xi \partial_\xi \left(\xi^2 a^2 R_0^2 \partial_r \xi \partial_\xi c \right) \\ &= \frac{D}{R_0^2} \frac{1}{a^2} \frac{1}{\xi^2} \partial_\xi (\xi^2 \partial_\xi c) \end{aligned} \tag{A.3}$$

Combining those expression give,

$$\partial_\tau c + \frac{a'}{a} \left(\frac{1}{\xi^2} - \xi \right) \partial_x i c = \frac{1}{\xi^2} \partial_x i (\xi^2 \partial_\xi c) \tag{A.4}$$

Where $a = da/dt$, this therm is proportional to the Peclet number $a' = \frac{\bar{R}R}{R_0 D} \sim Pe \ll 1$and therefore the terms with a' can be neglected.

Bibliography

[1] M. Amon and C. D. Denson. A study of the dynamics of foam growth: Analysis of the growth of closely spaced spherical bubbles. *Polymer Engineering and Science*, 24(13):1026–1034, 1984.

[2] C. B. Park and L. K. Cheung. A study of cell nucleation in the extrusion of polypropylene foams. *Polymer Engineering & Science*, 37(1):1–10, 1997.

[3] S. A. Thorpe. On the clouds of bubbles formed by breaking wind-waves in deep water, and their role in air-sea gas transfer. *The Royal Society*, 304, 1982.

[4] J.W. Westwater J.P. Glas. Measurements of the growth of electrolytic bubbles. *International Journal of Heat and Mass Transfer*, 7(12):1427–1430, 1964.

[5] T. van Terwisga B. Wieneke E. J. Foeth, C. W. H. van Doorne. Time resolved piv and flow visualization of 3d sheet cavitation. *Experiments in Fluids*, 40(4):503–513, 2006.

[6] S. Fang Z. Zhua. Numerical investigation of cavitation performance of ship propellers. *Journal of Hydrodynamics, Series B*, 24(3):347–353, 2012.

[7] W. L. Korff S. N. Patek and R. L. Caldwell. Biomechanics: Deadly strike mechanism of a mantis shrimp. *Nature*, 428:819–820, 2004.

[8] D. E. Yount and R. H. Strauss. Bubble formation in gelatin: A model for decompression sickness. *Journal of Applied Physics*, 47:5081–5089, 1976.

[9] C. Balestrad T.D. Karapantsiosc V. Papadopouloua, R.J. Eckersleyb and M-X Tanga. A critical review of physiological bubble formation in hyperbaric decompression. *Advances in Colloid and Interface Science*, 191:22–30, 2013.

[10] W. Yang. Dynamics of gas bubbles in whole blood and plasma. *Journal of Biomechanical Engineering*, 4:119–125, 1971.

[11] H. D. Van Liew and S. Raychaudhuri. Stabilized bubbles in the body: pressure-radius relationships and the limits to stabilization. *Journal of Applied Physiology*, 82:2045–2053, 1997.

[12] E.L. Jack A. Lachmann and D.H. Volman. Isothermal and isobaric degassing of ice cream. *Industrial & Engineering Chemistry*, 42(2), 1950.

[13] G.M. Evans S.F. Jones and K.P. Galvin. Bubble nucleation from gas cavities a review. *Advances in Colloid and Interface Science*, 80:27–50, 1999.

[14] J. S. McKechnie W. T. Lee and M. G. Devereux. Bubble nucleation in stout beers. *Physical Review E: Statistical, Nonlinear, and Soft Matter Physics*, 83:051609, 2011.

[15] A. N. Gent and D. A. Tompkins. Surface energy effects for small holes or particles in elastomers. *Journal of Polymer Science, Part B: Polymer Physics*, 7(9):1483–1487, 1969.

[16] D. Wang X. Zhang, D.Y. C. Chan and N. Maeda. Stability of interfacial nanobubbles. *Langmuir*, 13:1017–1023, 2013.

[17] J. H. Weijs and D. Lohse. Why surface nanobubbles life for hours. *Physical Review Letters*, 110, 2013.

[18] D. Lohse and X. Zhang. Pinning and gas oversaturation imply stable single surface nanobubbles. *Physical Review Letters*, 91, 2015.

[19] C. Voisin G. Liger-Belair and P. Jeandet. Modeling nonclassical heterogeneous bubble nucleation from cellulose fibers; application to bubbling in carbonated beverages. *Journal of Physical Chemistry B*, 109:1457314580, 2005.

[20] D. Lhse A. Prosperetti O.R. Enríquez, C. Sun and D. van der Meer. The quasistatic growth of CO_2 bubbles. *Journal of Fluid Mechanics*, 741, 2014.

[21] O.R. Enríquez. *Growing bubbles and freezing drops: depletion effects and tip singularities.* PhD thesis, Universiteit Twente, Enschede, 2015.

[22] P.S. Epstein an d M.S. Plesset. On the stability of gas bubbles in liquid-gas solutions. *Journal of Chemical Physics*, 18, 1950.

[23] M. Cable. The dissolving of stationay gas bubbles in a liquid. *Chemical Engineering Science*, 22:1393–1398, 1967.

[24] P.B. Duncan and D. Needham. Test of the epstein-plesset model for gas microparticle dissolution in aquous media: Effect of surface tension and gas undersaturation in solution. *Langmuir*, 20:2567–2578, 2004.

[25] Diran Basmadjian. *Mass transfer and separation processes; Principles and Applications*. CRC Group, 2007.

[26] G-W. Bruggert D. Lohse A. Prosperetti D. van der Meer O.R. Enríquez, C. Hummelink and C. Sun. Growing bubbles in a slightly supersaturated liquid solution. *Review of Scientific Instruments*, 84, 2013.

[27] S. Elghobashi I. Kim and W.A. Sirignano. On the equation for spherical particle motion: effet of reynolds and acceleration numbers. *Journal of Fluid Mechanics*, 367:221–253, 1998.

[28] D. L. Wiset and G. Hougton. Effects of an impermeable wall on bubble collapse in diffusion coefficient measurements. *Chemical Engineering Science*, 23:1501–1503, 1968.

Acknowledgements

Oscar and Devaraj, thank you for the opportunity to participate in this research and the patient guidance during the project. I want to thank the Physics of Fluid group for the good work place and the advanced equipment that I could use. Stefan thanks for providing the software that could acquire and process experimental data in real time and Javier for the theoretical derivation. Finally I want to thank my parents and grandparents for the great support during the whole process.